Co-modulation of synapses and voltage-gated ionic currents by combined actions of multiple neuromodulators follow distinct rules

Xinping Li, Dirk Bucher and Farzan Nadim

Federated Department of Biological Sciences, New Jersey Institute of Technology and Rutgers University-Newark, 323 Martin Luther King Blvd, Newark, NJ 07102

Acknowledgements: This work was supported by NIH Grants MH060605 and

Competing Interests: The authors declare no competing interests.

Figures: 8

Figure Supplements: 3

Abstract

Multiple neuromodulators continuously act in concert to shape the properties of neural circuits. Different neurmodulators can activate distinct receptors but have overlapping signaling pathways or targets through co-modulation. Mechanisms underlying circuit output and its functional consequences, therefore, depend on how neuromodulators interact on these shared targets, a process that is poorly understood. We explored the quantitative rules of co-modulation of two principal targets of neuromodulation, voltage-gated ionic currents and synaptic currents, in the pyloric circuit of the stomatogastric ganglion (STG) of the crab, Cancer borealis. The neuropeptides proctolin (Proc) and CCAP modulate STG synapses and converge to activate the voltage-gated ionic current IMI in multiple STG neurons. Using simultaneous voltage-clamp recordings from the reciprocally connected pyloric neurons PD and LP, we examined the validity of a simple dose-dependent quantitative rule that co-modulation by Proc and CCAP can be predicted as the linear sum of the individual effects of each modulator, up to saturation. We found that this rule is valid for the co-modulation of the synapses between these two neurons, but not for the activation of IMI, where co-modulation was found to be sublinear. Given the high level of evolutionary conservation of neuromodulator receptors and signaling pathways, such distinct rules for co-modulation of different components within the same neurons are likely to be common across neuronal circuits.

Introduction

All nervous systems adapt to changes in the environment and the internal state of the animal. In different contexts, awake or asleep, fed or hungry, light or dark, neuronal circuits produce different output (Xia and Mills, 2004; Inagaki et al., 2014; Wester and McBain, 2014; Burke et al., 2015; Filosa et al., 2016). This context-dependent output is actively shaped by various neuromodulators through changes in neuronal and synaptic properties (reviewed in Brezina, 2010; Bargmann, 2012; Marder, 2012; Nadim and Bucher, 2014). The large number of neuromodulators identified within species clearly indicates that, at any time, every neuronal network is co-modulated by a number of these substances (Marder and Bucher, 2007; Taghert and Nitabach, 2012; van den Pol, 2012; Richter et al., 2014; Su et al., 2014). The combination and distribution of neuromodulators present depends on, and often is the means to, convey context (Cohn et al., 2015 ; Lovett-Barron et al., 2017; White et al., 2017). Consequently, essential behaviors such as breathing, sleeping, learning, and mating, as well as cognitive tasks, rely on combined actions of multiple neuromodulators (Doi and Ramirez, 2008; Woods et al., 2014; He et al., 2015; Yamazoe-Umemoto et al., 2015; Mena et al., 2016; Asahina, 2017; Donlea

et al., 2017). Thus, proper neuronal network function depends on specific combinations of neuromodulators, and how they act in concert.

While much is known about the actions of single neuromodulators, few studies have explored how multiple neuromodulators interact. Most of these studies have provided qualitative descriptions of altered output at the systems level (Brezina et al., 1996; Dickinson et al., 1997; Mesce et al., 2001; Thirumalai and Marder, 2002; Beliez et al., 2014). Only a handful of studies have explored the combined actions of neuromodulators on their direct targets, also mostly qualitatively (McCormick and Pape, 1990; Parker, 2000; Djokaj et al., 2001; Svensson et al., 2001; Park and Spruston, 2012; Garcia et al., 2015).

Neuromodulator targets fall into two categories: ionic currents, which shape neuronal excitability, and synapses, which determine network organization. In a single neuron, a single neuromodulator can have multiple subcellular targets (divergence) and multiple neuromodulators can have overlapping targets (convergence) (reviewed in Nadim and Bucher, 2014). Such patterns of divergence and convergence can result in complex co-modulatory effects on neuron and synapse function, and consequently network output.

To understand how co-modulation shapes the network output, it is important to characterize how co-modulation occurs at shared targets. Here we focus on convergent co-modulation of synapses and voltage-gated currents by exploring 1) if the combined actions of neuromodulators on a shared target can be predicted quantitatively from their individual actions, and 2) if co-modulation of synaptic and voltage-gated ionic currents in a neuron follows the same rule. For neuromodulators with converging signaling pathways, the most parsimonious prediction would be that their effects at a shared target simply add up linearly to produce a combined effect, up to the saturation level. However, such linear addition does not exclude the possibility that the modulators may each have a distinct dose-dependent effect on the target, or that the dynamics of target actions is complex and non-linear.

In this study, we used the pyloric circuit of the crab stomatogastric ganglion (STG) to examine whether the dose-dependent actions of two peptide neuromodulators on their targets can be predicted by the linear summation of their individual actions, up to saturation. Several peptides activate a voltage-gated ionic current (IMI, Golowasch and Marder, 1992; Swensen and Marder, 2000) in STG neurons, likely through converging signaling pathways from different receptors (Garcia et al., 2015; Gray et al., 2017). Some also modulate pyloric synapses (Thirumalai et al., 2006; Zhao et al., 2011; Garcia et al., 2015). We measured the influence of two peptide neuromodulators on both synaptic currents and on I_{MI}. Because the influence of the peptides on these components can be assayed simultaneously, they provide a good test for understanding the rules of co-modulation of different aspects of neuronal processing. We found that co-modulation of synaptic transmission and the voltage-gated current follows

distinct rules—a mechanism likely to be generalizable. The machinery underlying neuromodulation is evolutionarily well conserved and most receptors have homologs across invertebrate and vertebrate systems (Mirabeau and Joly, 2013; Lovett-Barron et al., 2017), and many neuromodulators share G-protein mediated signaling pathways (Doi and Ramirez, 2008). Thus, such distinct rules for co-modulation of different components are likely to be used in other neuronal networks and by other neuromodulators.

Results

We explored the peptide neuromodulation, by CCAP and Proc, of the reciprocal synapses between the pyloric dilator (PD) and lateral pyloric (LP) neurons, as well as the activation of I_{MI} in the LP neuron. The influence of these peptides on pyloric neurons and synapses can be assayed simultaneously, while all other neuromodulatory inputs are removed.

We began by quantifying the individual modulatory effects of CCAP and Proc on both synapses and I_{MI} in the LP neuron across a range of concentrations, ranging from subthreshold to saturation. These dose-dependent quantifications allowed us to build predictors of the modulatory effect of each individual modulator at any concentration.

We then characterized the effect of co-application of both peptides in two stages. First, we examined if co-modulation is history dependent by co-applying the peptides following exposure to either Proc or CCAP, as interactions between neuromodulators can depend the order of application and produce priming or gating (Dickinson et al., 1997; Svensson et al., 2001). Then, in separate experiments, we tested the effect of various combinations of the two peptides, applied at different concentrations, and compared the results with the predictions of the linear summation rule.

Dose-dependent effect of individual peptides on the synapses

We quantified the individual modulatory effects of CCAP and Proc in separate sets of experiments. In each experiment, we measured the effect of the peptide on both the LP to PD and the PD to LP synapses. Hence, we will discuss four different synapse-peptide cases: LP to PD-CCAP, LP to PD-Proc, PD to LP-CCAP and PD to LP-Proc.

In each synapse-peptide case, we measured the postsynaptic current in control and in increasing concentrations of the peptide with simultaneous two-electrode voltage clamp recordings of both neurons (Figure 1A). In the STG, two identical PD neurons and the AB neuron are strongly electrically coupled and form the pacemaker group. Unless specified otherwise, the PD to LP synapse in this study refers to the combined synaptic current from the pacemaker group to the LP neuron. As expected for a graded synapse, the amplitude of postsynaptic

current increased as the presynaptic step voltage increased (Figure 1B and C). The current-voltage relationship of each synapse was fit with the sigmoidal curve given by equation (1), which is described by three parameters: I_{max} (synaptic amplitude), V_{mid} (half-activation voltage) and V_c (slope factor at V_{mid}). A more positive V_{mid} indicates a higher threshold for activation and larger V_c means a shallower activation curve (Figure 1D). For each synapse-peptide pair, we examined how I_{max}, V_{mid} and V_c were changed by the peptides (Figure 2).

For the LP to PD synapse, both CCAP and Proc significantly increased I_{max}, shifted V_{mid} to more negative potentials, and reduced V_c across concentrations (Figure 2A). In contrast, for the PD to LP synapse, CCAP only increased I_{max}, but did not affect V_{mid} or V_c, while Proc only decreased V_c, but did not affect I_{max} or V_{mid} (Figure 2B).

Notably, the same peptide modulated different synapses differently (e.g., I_{max}, V_{mid} and V_c were changed for the LP to PD-CCAP pair but only I_{max} for PD to LP-CCAP pair). Also, different peptides modulated the same synapse differently (e.g., CCAP modulated I_{max} while Proc modulated V_c for the PD to LP synapse.) Overall, both CCAP and Proc strengthened both synapses, although the manner of modulation depended on the synapse and the modulator.

We used the data shown in Figure 2 to build predictors for each synapse-peptide pair. The predictor is a surface fit to all synaptic current amplitudes, measured at different presynaptic voltage steps and modulation concentrations (Figure 3), which has a sigmoidal relationship with both the presynaptic voltage and the modulator concentration (fit given by equation (3)). These predictors allow us to estimate the synaptic current at any voltage and modulator concentration by interpolation. The surface fits also allow us to visualize and measure the distinct modulation effects of the two peptides on each synapse and of each peptide on the two synapses.

The saturation level of the co-modulatory effect on the synapses is not history dependent

Our main hypothesis assumes that the saturation of synaptic co-modulation is not affected by the order of application; that is, one modulator does not gate or prime the effect of the other modulator. Prior to testing our hypothesis, it was therefore important to verify this assumption. To test if the co-modulatory saturation level depended on the prior application of either modulator, we did two separate sets of experiments for each synapse. In each experiment, we saturated the synapse with either Proc or CCAP first, and then with both peptides co-applied.

Saturation of the neuromodulatory effects can occur when the receptors, the signaling pathways, or the targets themselves reach maximum capacity. Whether co-modulation has a larger effect compared to the effect of a single neuromodulator depends on which of these three is the limiting factor. If the limiting factor is the target, each modulator should occlude

the effect of the others, wheraeas if the limiting factor is the receptor, neither modulator should occlude the others. If the signaling pathways limit the saturation, occlusion would depend on the pathway interactions.

We first examined if co-modulation produced an additional effect above that of the single neuromodulator at 1 µM, the presumed saturation concentration of peptide effects in the STG (Zhao et al., 2011). In only one of the four cases, co-modulation increased the effect. For the PD to LP synapse, Proc did not completely occlude the effect of adding CCAP, probably because Proc receptors alone do not fully activate the target. In the other three cases, co-application did not produce an additional effect (Figure 4). The fact that complete occlusion was achieved in both synapses by at least one peptide, comfirms that the saturation level of the synaptic current was achieved by co-applying 1 µM CCAP and Proc. (It is possible, however, that other modulators could further enhance the synaptic currents.)

Notably, for both the LP to PD and the PD to LP synapses, the co-modulation saturation level does not depend on which peptide was applied prior to co-modulation (Figure 4). We also verified that the control measurements were the same for each synapse. Therefore, although co-modulation may have additional effects depending on the neuromodulator and the synapse, the saturation level of synaptic co-modulation was not history dependent.

Neither CCAP nor Proc modulates short-term synaptic plasticity

The pyloric circuit is rhythmically active with a frequency between ~0.5 and 2 Hz (Goaillard et al., 2009). Like many synapses in the STG, the LP to PD and PD to LP synapses exhibit short-term synaptic depression (Tseng and Nadim, 2010; Zhao et al., 2011). In rhythmically active circuits, short-term synaptic plasticity means that the strength of the synapse depends on the period of the rhythm (Manor and Nadim, 2001). This means that depressing synapses are the stronger the faster the rhythm is, whereas the opposite is true for facilitating synapses. Hence, neuromodulation of short-term synaptic plasticity can play an important role in shaping circuit output and dynamics.In the LP to PD synapse, short-term synaptic dynamic can change in the presence of Proc, dependent on the amplitude of presynaptic voltage change (Zhao et al., 2011).

For both synapses, neither CCAP, nor Proc, nor co-application of both significantly changed the level of short-term synaptic depression (Figure 5). This result, obtained with 40 mV amplitude voltage steps, is consistent with a previous report of the effect of Proc on the LP to PD synapse (Zhao et al., 2011). When much smaller presynaptic steps were used in that study, Proc did change short-term plasticity. It is possible that differences in short-term plasticity may exist, depending on the presynaptic voltage range (Zhao et al., 2011). However, a detailed analysis of the voltage-dependence of modulatory effects on synaptic plasticity exceeded the scope of our study.

Co-modulatory effects on synapses are linearly additive up to saturation

After establishing that the saturation level of co-modulation is not history dependent, we used equation (6) to calculate the co-modulation predictions for the synapses. Recall that the individual effects of the two peptides were modeled by the predictors for their dose-dependent effects (equation (3)and Figure 3). The linear summation rule predicts that the co-modulatory effect is the sum of the individual modulatory enhancements due to Proc and CCAP at their respective concentrations (equation (4)), up to saturation. We tested this prediction on the LP to PD and the PD to LP synapses with 18 different co-modulation combinations (see Methods).

We compared our predictions with the experimental results by computing the coefficient of determination (R^2, evaluating the trend of the data) and normalized root mean squared error (NRMSE, evaluating the deviation of the data from the prediction; see Methods). We report these statistics for each combination individually and also report the overall R^2 and NRMSE for all combinations.

For the LP to PD synapse, our prediction matched the experimental results very well (Figure 6A, not all cases are shown, but all data are provided in Figure 6-source data). The comparison between predicted and measured values at all data points showed high prediction accuracy (Figure 6B, the line y=x indicates a perfect match). For all combinations, we obtained high R^2 and low NRMSE values, indicating that our predictions both captured the trend of the data well and had negligible deviation from the data (Figure 6C; see Figure 6-figure supplement for exact values). The overall values were $R^2 = 0.90$ and NRMSE = 0.31 for this synapse. We therefore concluded that co-modulation of LP to PD synapse can be predicted from effects of individual peptides using the linear summation rule.

We observed simililar accuracy of the linear prediction for the PD to LP synapse (Figure 7A, not all cases are shown, but all data are provided in Figure 7-source data). The predictions for the PD to LP synapse also had high R^2 and low NRMSE with overall $R^2 = 0.73$ and NRMSE = 0.52 (Figure 7B and C; see Figure 7-figure supplement for exact values. Although the the prediction was not as accurate as that of the LP to PD synapse, these values still indicated that co-modulation of the PD to LP synapse was predicted well using the linear summation rule.

Co-modulatory effects on I_{MI} are not linearly additive

Our data indicate that the co-modulatory effects of Proc and CCAP on the synapses are linearly additive, up to saturation. This suggests that the intracellular pathways underlying the Proc and CCAP effects converge in the LP and PD neurons, without additional interactions. If so, it is reasonable to assume that the activation of I_{MI} by Proc and CCAP would also follow the same rule.

226 The protocols that we used to measure the synaptic current from LP to PD also allowed us to
227 estimate the level of I_{MI} in the LP neuron (see Methods and Figure 8A). We therefore quantified
228 the dose-dependent levels of I_{MI} in the presence of either Proc or CCAP. Both peptides activated
229 I_{MI} starting at nanomolar concentrations and consistently produced larger currents as the
230 concentration increased (Figure 8B and C).

231 In each experiment, either Proc or CCAP was applied at increasing concentrations up to 1µM,
232 and then both peptides were co-applied at 1 µM each to estimate the co-modulation I_{MI}
233 saturation level. As with the synapses, the saturation level did not depend on whether Proc or
234 CCAP was applied first, before co-application (Figure 8C).

235 The dose-dependent curves for the two peptides were used to construct the predictors of the
236 co-modulation effect (equation (5)). From these individual predictors, we calculated the I_{MI}
237 levels expected to be activated by each peptide at any concentration, using linear summation
238 to saturation (equation (7)). As with the synapses, we compared the predicted I_{MI} levels to the
239 actual measurements in 18 different co-modulation combinations. We then calculated the R^2
240 and NRMSE values for each individual combination and for all combinations together. For these
241 comparisons, I_{MI} was measured at -15 mV. Calculations of the R^2 and NRMSE values with the
242 peak I_{MI} level, derived from the fitted IV curves (equation (2)), produced similar results
243 (provided in Figure 8-source data).

244 Surprisingly, in contrast to the synapses, our predictions were far from the measured values of
245 the co-modulated I_{MI} in the LP neuron (Figure 8E top). The comparison between predicted and
246 measured I_{MI} value showed over-estimation in most of the data points (Figure 8D). For half of
247 the combinations, R^2 values was below 0 and NRMSE values were above 1 (Figure 8E middle;
248 see Figure 8-figure supplement for exact values). The low overall R^2 value of 0.08 and high
249 overall NRMSE value of 0.96 indicate that our linear summation model was a very poor
250 predictor for the co-modulation of I_{MI} and in fact no better than using the mean of the data as a
251 predictor.

252 Interestingly, also in contrast to the fairly consistent R^2 and NRMSE values across different co-
253 modulation combinations for the synapses, these values varied drastically across different
254 combinations for I_{MI} (Figure 8E middle). The predictor did a very poor job (NRMSE>1) when at
255 least one of the peptide had a low concentration, but a somewhat better job (NRMSE closer to
256 0) when the combined concentrations were high, mostly because the predictor estimated the
257 co-modulation to be at saturation (Figure 8E).

258 Despite the poor prediction, our linear model provided some useful information about the
259 dynamics of I_{MI} co-modulation. The measured I_{MI} level was always lower than the prediction,
260 indicating that the co-modulatory effect was sublinear.

Discussion

Distinct rules for co-modulation of different intercellular targets

Understanding the rules of co-modulation of neural circuit components is a necessary first step towards unraveling how co-modulation affects circuit output. Co-modulation of neuronal excitability and synaptic transmission by multiple substances means that circuit output depends on the degree to which different receptors converge on the same signaling pathways, or how separately activated signaling pathways interact. It is common for multiple neuromodulators to target the same ion channel or synapse, and multiple neuromodulators can also converge on different targets in the same neuron (McCormick 1989, Harris-Warrick 2011)(Marder, 2012). It is crucial to understand if convergent neuromodulators act in a simple additive manner or display more complex, nonlinear interactions. The actions of converging neuromodulators may have the same or opposing signs (Nadim and Bucher, 2014). If two modulators influence the same component with the same sign, their co-modulatory effect could be additive, synergistic (priming), or antagonistic. Even if they have opposite effects when applied separately, co-application could reveal additive interactions or lead to more complex nonlinear outcomes. If two modulators converge onto multiple intracellular targets, an open question remains if their interactions follow the same rule at all targets.

Despite recent advances in genetic and imaging tools (Arrigoni and Saper, 2014; Cohn et al., 2015; Shahidi et al., 2015), many systems still lack experimental accessibility or the basic understanding of neuromodulator actions on their cellular and subcellular targets to explore this topic. Peptide neuromodulation of the pyloric circuit of the STG provides a special opportunity to explore the rules of co-modulation of synaptic and intrinsic ionic currents, and to understand their consequences at the circuit level. We observed linearly additive co-modulation of synapses, but sub-linearly additive co-modulation of a voltage-gated ionic current in the same neurons. These specific results may be idiosyncratic for the neurons and synapses we studied, as co-modulation of synapses can be nonlinear (Parker, 2000), and it is plausible that co-modulation of voltage-gated ionic currents could be linearly additive. However, the important lesson from our findings is that converging co-modulation of synapses and ionic currents, or different subcellular targets in general, can follow distinct rules. Given the complex patterns of divergence and convergence of neuromodulators in many systems, this finding likely has broad functional implications.

Linearly additive co-modulation of pyloric synapses

Modulation of synaptic currents may involve both presynaptic changes in transmitter release and postsynaptic changes in ionotropic receptor properties. Therefore, the total effect can

result from modulation of molecular components in two different neurons, involving potentially distinct signaling pathways and concentration-dependence. At synapses in the STG, this is exemplified by the finding that a single neuromodulator can exert functionally opposing effects on the pre- and postsynaptic sides (Garcia et al., 2015)(Harris-Warrick & Johnson 2010). We therefore did not necessarily expect co-modulation of synapses to be simply linearly additive. Surprisingly, we observed such linearly additive co-modulation at both synapses. For the LP to PD synapse, CCAP modulation must be pre-synaptic, as PD neurons do not express CCAP receptors (Garcia et al., 2015). However, Proc modulation could have both pre- and post-synaptic components. Although Proc receptor expression in these neurons has not been tested because their molecular identity has not been determined in the STG, both neurons show IMI activation in response to Proc application (Swensen and Marder, 2000). For the PD to LP synapse, both modulators could have pre- and post-synaptic effects. The synaptic input to the LP neuron from the pacemaker (which we measured as the PD to LP synapse) is from both AB and PD neurons. AB expresses CCAP receptors (Garcia 2015) and isolated AB neurons respond to both CCAP and Proc (Swensen 2001). The fact that we measured the synaptic responses of LP while voltage clamping only one of the presynaptic neurons may explain why linear summation less accurately predicts co-modulation compared to the LP to PD synapse (Figures 6 and 7).

For both synapses and both neuropeptides, we did not investigate whether modulatory effects occured pre- or post-synaptically, or on both sides. However, given that we found linear summation and occlusion, it is likely that modulatory signaling on either side was purely converging, without any nonlinear interactions. Linear co-modulation could also occur through spatial segregation, for example because one neuromodulator only acted presynaptically, and the other only postsynaptically. Even in a single neuron, modulatory microdomains can provide non-overlapping, independent activation of identical targets, even when the same signaling pathways are used (Lur & Higley 2015). However, in the case of spatial segregation, no occlusion should occur and the saturation level of co-modulation should be the linear sum of the maximum effects achieved by each neuromodulator.

Sublinear co-modulation of I_{MI}

In contrast to the synapses, we observed nonlinear co-modulation of IMI, which indicated that the signaling pathways targeting IMI were distinct from the pathways targeting the synapses. It was previously hypothesized that peptides may modulate synapses in the STG through their actions on the IMI channel, which was speculated to be partially permeable to calcium (Zhao et al., 2011; Gray et al., 2017). However, our results indicate that this is unlikely, given that linear co-modulation of the synapses and nonlinear co-modulation of IMI were observed in the same experiments. In addition, the nonlinearity of IMI co-modulation may have two components: sublinear interactions when at least one modulator is at low concentration, occlusion when

both are at high concentrations (Figure 8E). The occlusion effect was also shown in our previous study (Garcia et al., 2015).

Interestingly, in other decapod species, at least two subtypes of CCAP receptors are found, which have very different efficacies ((EC 50 of 30+ folds difference Li et al., 2011). A similar mechanism may be at play in our system where peptides activate IMI through receptor subtypes with different affinities. If so, the low- and high-affinity pathways mediated by the same peptides should undergo simple convergence, so that the dose-dependent activation of IMI is sigmoidal (Figure 8C). Similarly with the low-affinity receptor mediated pathways of both peptides, hence the occlusion at high concentrations. However, the high-affinity pathway mediated by one peptide might interfere with the low-affinity pathway mediated by the other, possibly by targeting the intracellular calcium concentration or calcium-binding proteins (Gray et al., 2017). Another possible mechanism is that the CCAP and Proc receptors can form a heteromer complex and display behaviors distinct from either receptor alone (reviewed in Smith and Milligan, 2010). Given the potential mechanisms possible, a different set of experiments as well as mathematical modeling is required to provide an accurate description of the co-modulation rule for IMI.

Distinct co-modulation rules may increase flexibility and functionally uncouple the modulation of different targets

If the actions of multiple neuromodulators on shared targets are similar and sum up linearly, the co-modulatory effects mainly depend on the concentrations and the saturation level. However, by having different co-modulation rules for different targets, co-modulation can produce a different effect than each individual neuromodulator, thus providing an extra degree of freedom. In such a case, degeneracy is present at the target level, as the effect of each neuromodulator can be replaced by the other, yet additional flexibility is achieved at the output level.

When different neuromodulators converge onto multiple targets, their actions on the shared targets are inextricably linked. However, modulator effects can be uncoupled by different co-modulation rules. For example, in the results shown here, 1 nM CCAP and 100 nM Proc produced an additive effect in the LP to PD synapse, but activated much less IMI than 100 nM Proc alone (Figures 6A, 8C and 8E).

In the pyloric circuit, IMI enhances neuronal excitability of the pacemaker neurons and thereby regulates the pyloric frequency (Hooper and Marder, 1987). The synapses from the pacemaker neurons (AB and PD) to follower neurons like LP are important for the regulation of burst phasing across pyloric neurons (Goaillard et al., 2009), and the feeback synapse from LP to PD stabilizes network frequency (Zhao et al., 2011). Distinct rules for co-modulation of neuronal excitability and synaptic interactions could functionally uncouple these effects and

therefore allow burst phasing and rhythm frequency to be regulated differentially. Additionally, sub-linear co-modulation of IMI may extend the dynamic range for the modulation of neural excitability. Because STG neurons are modulated by many peptides, sublinear co-modulation would ensure that neuronal excitability is not saturated during baseline activity when many peptides may be present at low concentrations. Yet, when any specific peptide neuromodulator is released at a higher concentration, it can produce a distinct circuit output.

Co-modulation in light of animal-to-animal variability

Across individuals, pyloric neurons display substantial variability in the magnitude of synaptic and voltage-gated ionic currents, as well as in the expression levels of mRNAs that code for ion channels (Golowasch 1999; Schulz 2006,2007; Goaillard 2009). Despite this variability, which is several-fold in some cases, neuronal excitability and the patterning of circuit activity is well maintained (Bucher 2005, Goaillard 2009). Substantial variability has also been described for neuromodulatory components. For example, CCAP receptor mRNA expression varies 3-fold in LP neurons (Garcia 2015), and CCAP-activated IMI in LP varies more than 5-fold in amplitude (Goaillard 2009). There may also be long-term regulatory changes in neuromodulation, perhaps due to seasonal or molt cycle related hormonal changes. In contrast to the data presented here, we found in a previous study that in LP, CCAP activated a larger IMI than Proc did, and the Proc response was not saturating (Garcia et al., 2015). However, circuit modulation is at least qualitatively consistent enough to elicit modulator-specific activity patterns that are similar across individuals, and at different times during the year. In the current study, we did not measure responses to co-modulation in a large enough sample to report meaningfully the extent of variability. However, we note that even with our small sample size, the co-modulation effects were consistent. Therefore, co-modulation rules appear to be robust across individuals, despite component variability.

Remaining questions

Unraveling the consequences of co-modulation at the circuit level requires examining their interactions at multiple levels. In this study, we took a first step toward identifying the rules of co-modulation at the level of shared targets. However, our study leaves several questions unanswered. First, the second messenger pathways resulting in our observed data remain unknown. Other model systems, in which the subcellular pathways are well understood, would be better suited to examine the signaling pathway interactions of neuromodulators.

Second, in our study we bath applied neuromodulators, which was a necessary step to quantify precise dose-dependent effects, but as a number of studies in the STG have shown, fails to address the spatiotemporal dynamics of neuromodulation (Nusbaum et al., 2017). Neuromodulators can be released as hormones or as neurotransmitters. In latter case, spatiotemporal properties of synaptic transmission can be critical in determining circuit output

(reviewed in Nusbaum et al., 2017). The temporal dynamics of the neuromodulatory effects of neurotransmitters is, by necessity, determined by the patterns of activity of the modulatory neurons that release these transmitters. Interestingly, the activity patterns of the modulatory projection neurons in the STG (and other systems) is subject to feedback from the activity of the target circuits, thereby producing another potential level of complexity. The spatial interactions depend on the architecture of the local circuits, the spatial pattern of neuromodulator release and the peptidase activity. To probe the spatiotemporal dynamics of co-modulation, combining experimental approaches, such as stimulating neuromodulatory projection neurons, and computational modeling is necessary.

Finally, all our experiments were done with voltage-clamp steps in order to characterize the neuromodulatory effects on each target. However, such experiments mask the interactions among circuit components, both those within neurons and those with their synaptic partners. One such example is shown in (Zhao et al., 2011) for the LP to PD synapse, where Proc changes two factors: it enhances both the burst voltage waveform of the presynaptic LP neuron and the amplitude of the synaptic current. When the LP neuron is voltage clamped with the pre-recorded realistic control or Proc voltage waveforms, the resulting synaptic currents are similar in control saline, but different in the presence of Proc. This indicates that the first factor (change in the LP waveform) only produces a meaningful effect only in conjunction with the second factor (direct enhancement of synaptic release). Exploring such interactions among cellular or circuit components is important in understanding the functional consequences of co-modulation and requires further experiments and computational modeling.

Conclusions

Neural systems are continuously subjected to neuromodulatory chemicals, released locally, by projection pathways and as hormones. At this stage in the progression of neuroscience, it is an accepted fact that these neuromodulatory chemicals are necessary for the normal function of neural circuits and their presence and patterns of release alters the output of these circuits. It follows logically that understanding the rules of interaction among neuromodulators has clear relevance for understanding circuit dynamics and the resulting behaviors. Identifying the mechanisms of co-modulation also provides mechanistic guidance for therapies that target one or more neuromodulatory pathways (Engineer et al., 2011; Pena et al., 2014; Freret et al., 2017). Our results show the feasibility of a quantitative description of co-modulation rules at the target level, and provide a framework that can be extended to other circuit components and other neuromodulators in the STG and in other systems. Achieving this goal, however, requires a systematic approach to understand co-modulation at multiple levels, to dissect complex interactions among neuromodulators and between these modulators and their targets, to describe the nonlinear interactions between the co-modulated components to describe changes in circuit output, and to bridge gaps of knowledge using multiple model systems.

Materials and Methods

Preparation and electrophysiological recordings

All experiments were done on wild-caught adult male crabs (*Cancer borealis*) purchased from local seafood stores. Prior to experiments, animals were kept in artificial sea water tanks at 13 °C. Before dissection, crabs were anesthetized by placing on ice for at least 30 min. The STNS was dissected out following standard protocols (Blitz et al., 2004; Tohidi and Nadim, 2009), placed in a Petri dish coated with clear silicon elastomer (Sylgard 184; Dow Corning; Midland, MI) and superfused with *Cancer borealis* saline, containing (in mM) 11 KCl, 440 NaCl, 13 $CaCl_2$, 26 $MgCl_2$, 11.2 Trizma base, and 5.1 maleic acid (pH =7.4 –7.5). A petroleum jelly well was built around the STG for constant superfusion of chilled (10-12 °C) saline during the experiment.

For neuron identification, extracellular motor nerve recordings were obtained with a differential AC amplifier (A-M Systems, Model 1700; Sequim, WA), using stainless-steel pin wire electrodes placed inside and outside of small petroleum jelly wells built around the nerves. Intracellular recordings and voltage clamp were done with Axoclamp 900A amplifiers (Molecular Devices; San Jose, CA). The STG was desheathed and the neuron somata were impaled with sharp glass electrodes, pulled with a Flaming-Brown P-97 Puller (Sutter Instruments; Novato, CA) and filled with 0.6 M K_2SO_4 + 20 mM KCl solution (15-30 MΩ electrode resistance). Neurons were identified by their characteristic intracellular waveforms and by matching their activities to the spikes on the corresponding motor nerves. All electrophysiological data were digitized at 5-10 KHz with a Digidata 1440A data acquisition board (Molecular Devices).

Neuromodulatory effects on the strength and dynamics of the synaptic currents

The neuromodulatory effects on strength and short-term plasticity of the graded component of both the LP to PD and the PD to LP synapses were measured with simultaneous dual two-electrode voltage clamp recordings of the PD and LP neurons.

In voltage clamp experiments, 10 nM tetrodotoxin citrate (TTX; Biotium; Fremont, CA) saline was bath applied to block action potentials and descending neuromodulatory inputs. The synaptic current was measured as the current elicited in the postsynaptic neuron (held at –50 mV), in response to depolarizing 500-1000 ms voltage steps in the presynaptic neuron (from a holding potential of –60 mV to 0 mV, in 10 mV steps; Figure 1 B and C). The postsynaptic current reported in this study is the mean value of the current during the first 500 ms of the presynaptic pulse (the postsynaptic current integral divided by the presynaptic voltage step

duration of 500 ms). The peak values of the synaptic currents during each voltage step are included in Figure 2–source data.

To fit the postsynaptic current amplitude as a function of presynaptic voltage (V_{pre}), we used a sigmoid function of the following form:

$$I_{syn} = \frac{I_{\max}}{1+\exp\left(-\frac{V_{pre}-V_{mid}}{V_c}\right)} \quad (1)$$

In these fits, we assumed that the postsynaptic current was 0 at V_{pre} = -70 mV.

Proc (Bachem; Torrance, CA and Genscript; Piscataway, NJ) and CCAP (Bachem) were aliquoted in 1 mM M stock solutions and stored at -20 °C until use. For each experiment, the aliquots were further diluted to the desired concentrations. The dose-dependent effect of Proc or CCAP on synapses was measured by bath applying each peptide from low to high concentration (1 nM to 1 µM) with a four-minute interval between each concentration. We considered 1 µM to be the saturation concentration of both Proc and CCAP based on previous studies (Zhao et al., 2011). In addition, 1µM Proc and CCAP were co-applied at the end of each experiment to measure the maximum modulatory effect.

To measure short-term synaptic plasticity, we voltage clamped the presynaptic neuron at a holding potential of -60 mV and applied a set of five 500 ms identical depolarizing square pulses, from -60 to -20mV, at 1Hz. We measured the mean current amplitude in the postsynaptic neuron (voltage clamped at -50 mV) in response to each pulse. The level of short-term plasticity was quantified as the ratio of the postsynaptic current amplitude elicited by the fifth and first pulses. For the experiments that had two repeated measurements, we averaged the two measurements.

Neuromodulatory effects on the voltage-gated ionic current I_{MI}

The modulator-activated inward current I_{MI} was measured in the LP neuron in the same experiments in which we measured the LP to PD synaptic current. Because, in these experiments, the LP neuron membrane potential was stepped from -60 to 0 mV for measuring the LP to PD synapse (using the current measured in the postsynaptic PD neuron), the same voltage steps could be used to estimate I_{MI} in the LP neuron (using the voltage-clamp current, I_{LP}, injected in the presynaptic LP neuron). I_{MI} was measured as the difference between I_{LP} measured in the presence of the modulator and I_{LP} measured in control saline (Figure 8A) (Golowasch and Marder, 1992). I_{MI} is a non-inactivating current (Golowasch and Marder, 1992; Gray et al., 2017). To reduce errors due to differences in transient currents, we reported the mean value of the difference current, measured in the second half of each voltage pulse where

the currents had reached approximate steady state. The I_{MI} value at -15 mV was measured as the average of the currents elicited at -20 mV and -10 mV step voltage and used for analysis.

I_{MI} is a non-inactivating fast voltage-gated inward current whose activation curve is a simple Boltzmann sigmoidal equation (Goaillard et al., 2009). The IV curve of IMI can therefore be estimated as

$$I_{MI} = \frac{g_{\max}(V_{LP} - E_{MI})}{1 + \exp\left(-\frac{V_{LP} - V_{mid}}{V_c}\right)} + I_0 \qquad (2)$$

where g_{max} is the maximum conductance of I_{MI}, E_{MI} is the reversal potential and I_0 is the baseline difference current.

The dose-dependent effects of the modulators and the protocols for co-modulation of I_{MI} were the same as those described for the synapses above.

Constructing predictors for single neuromodulators

For each neuromodulator-synapse pair, we fit a surface to the postsynaptic currents measured at all presynaptic voltages and concentrations in multiple experiments. The equation used to define this surface was a dual sigmoidal function of both the presynaptic voltage (V_{pre}) and the log peptide concentration (C). This equation was based on equation (1), so that

$$I(V_{pre}, C) = \frac{I_{\max}(C)}{1 + \exp\left(-\frac{V_{pre} - V_{mid}(C)}{V_c(C)}\right)}, \text{ where,}$$

$$I_{\max}(C) = a_1 + \frac{a_2}{1 + \exp\left(\frac{C - C_{mid}}{C_c}\right)}$$

$$V_{mid}(C) = a_3 + \frac{a_4}{1 + \exp\left(\frac{C - C_{mid}}{C_c}\right)} \qquad (3)$$

$$V_c(C) = a_5 + \frac{a_6}{1 + \exp\left(\frac{C - C_{mid}}{C_c}\right)}.$$

In these fits, the unit of peptide concentration is M, and the control value was set at C = -10, thus assuming that 10^{-10} M concentration had no effect. The enhancement functions for each peptide were defined as the increase produced by the modulator above the control level of the synaptic current at each presynaptic voltage:

$$E(V_{pre}, C) = I(V_{pre}, C) - I_{Ctrl}(V_{pre}) \quad (4)$$

The resulting enhancement functions served as predictors for the effect of the neuromodulator on the postsynaptic current at any voltage and concentration.

In the case of I_{MI}, we fit the dose-dependent effects of Proc and CCAP with the sigmoidal curve

$$I_{MI} = \frac{I_{\max}}{1 + \exp\left(-\frac{C - C_{mid}}{C_c}\right)} \quad (5)$$

where C is the log peptide concentration and C_{mid} and C_c are, respectively, the half-maximum log concentration and the slope factor. In these fits, the unit of peptide concentration is M, and the control value was set at C = -10, assuming that 10^{-10} M concentration had no effect.

Predicting and testing co-modulation

We compared the predictions of co-modulation effects with the experimental data from co-applications of Proc and CCAP in 18 different combinations of concentrations for both the LP to PD and PD to LP synapses and I_{MI} in the LP neuron. These 18 combinations were divided into four separate groups of experiments, with each group only containing four or five combinations (group information can be found in Figure 6- Figure supplement). In each group of experiments, each peptide was applied in order from lower to higher concentration. Each combination was bath applied for a four-minute-interval, a value calculated by the superfusion rate, the volume of solution in the line and the size of the petroleum jelly well around the STG. At the end of each experiment, Proc and CCAP were co-applied at 1 µM each to record the maximum modulatory effect in that preparation.

The predictions for synapses were calculated by adding up the enhancements produced by each peptide at the respective concentrations (obtained from equation (4)) and the control value ($I_{Ctrl_co-\mathrm{mod}}$), and limiting the sum to the saturation level ($I_{sat_co-\mathrm{mod}}$), which is the synaptic current elicited by both peptides co-applied at 1µM.

$$I_{co-mod} = \begin{cases} E_{Proc} + E_{CCAP} + I_{Ctrl_co-mod} & \text{if} \le I_{sat_co-mod} \\ I_{sat_co-mod} & \text{otherwise} \end{cases} \quad (6)$$

For each combination, we measured the co-modulated synaptic currents, as described above, at presynaptic voltages from -60 mV to 0 mV, in 10 mV steps. We then compared the measurement with the prediction for those voltages.

The co-modulation predictions for I_{MI} were calculated by simply adding up the value of I_{MI} activated by each modulator at its respective concentration on the dose-response curve, limited to the saturation level.

$$I_{MI-co-mod} = \begin{cases} I_{MI-Proc} + I_{MI-CCAP} & \text{if} \le I_{sat_co-mod} \\ I_{sat_co-mod} & \text{otherwise} \end{cases} \quad (7)$$

To estimate how well our model prediction fit the experimental results, we used two standard goodness-of-fit tests. One of these measures is the coefficient of determination R^2 measured as: $R^2 = 1 - \frac{SSR}{SST}$, where $SSR = \sum_{i=1}^{n} (pred_i - meas_i)^2$ is the summed square of the residuals and $SST = \sum_{i=1}^{n} (meas_i - meas_{avg})^2$ is the total sum of squares. $R^2 = 1$ means that the prediction perfectly captures the trend of the data. Note, however, that this R^2 is different from the Pearson correlation coefficient where a linear fit to the data is evaluated. In our case, R^2 may be < 0, which simply indicates that the mean of the data $meas_{avg}$ provides a better prediction than the model.

The second measure we use is the normalized root mean squared error (NRMSE, normalized to standard deviation), calculated as $NRMSE = \frac{1}{\sigma_{meas}} \sqrt{\frac{SSR}{n}}$. A value of 0 for NRMSE indicates a perfect fit, whereas values > 1 indicate that the mean of the data $meas_{avg}$ provides a better prediction than the model.

We report both R^2 and NRMSE as recommended by Schunn and Wallach (Schunn and Wallach, 2005) to show that our prediction captures both the trend of the data and how far it deviates from the exact data points. Specifically, R^2 evaluates whether the model prediction captures the trend of the data, whereas, NRMSE evaluates the deviation of the data from the prediction.

Data analysis and statistical analysis

All data and statistical analysis were done with Matlab (MathWorks, 2015b; Natick, MA) and R (The R Foundation). Unless otherwise indicated, all error bars represent standard error of the mean. Statistical tests included Student's t-test, One- or Two-way RM ANOVA (followed by post hoc pairwise comparisons done with the Tukey method, when applicable). Critical significance level was set to α=0.05. Comparisons between model prediction and the data were done by reporting the adjusted R^2 and normalized root mean square error (NRMSE) analysis, as described above.

References

Arrigoni E, Saper CB (2014) What optogenetic stimulation is telling us (and failing to tell us) about fast neurotransmitters and neuromodulators in brain circuits for wake-sleep regulation. Curr Opin Neurobiol 29:165-171.

Asahina K (2017) Neuromodulation and Strategic Action Choice in Drosophila Aggression. Annu Rev Neurosci 40:51-75.

Bargmann CI (2012) Beyond the connectome: how neuromodulators shape neural circuits. Bioessays 34:458-465.

Beliez L, Barriere G, Bertrand SS, Cazalets JR (2014) Multiple monoaminergic modulation of posturo-locomotor network activity in the newborn rat spinal cord. Front Neural Circuits 8:99.

Blitz DM, Beenhakker MP, Nusbaum MP (2004) Different sensory systems share projection neurons but elicit distinct motor patterns. J Neurosci 24:11381-11390.

Brezina V (2010) Beyond the wiring diagram: signalling through complex neuromodulator networks. Philos Trans R Soc Lond B Biol Sci 365:2363-2374.

Brezina V, Orekhova IV, Weiss KR (1996) Functional uncoupling of linked neurotransmitter effects by combinatorial convergence. Science (New York, NY) 273:806-810.

Burke PG, Kanbar R, Basting TM, Hodges WM, Viar KE, Stornetta RL, Guyenet PG (2015) State-dependent control of breathing by the retrotrapezoid nucleus. J Physiol 593:2909-2926.

Cohn R, Morantte I, Ruta V (2015) Coordinated and Compartmentalized Neuromodulation Shapes Sensory Processing in Drosophila. Cell 163:1742-1755.

Dickinson PS, Fairfield WP, Hetling JR, Hauptman J (1997) Neurotransmitter interactions in the stomatogastric system of the spiny lobster: one peptide alters the response of a central pattern generator to a second peptide. J Neurophysiol 77:599-610.

Djokaj S, Cooper RL, Rathmayer W (2001) Presynaptic effects of octopamine, serotonin, and cocktails of the two modulators on neuromuscular transmission in crustaceans. J Comp Physiol A 187:145-154.

Doi A, Ramirez JM (2008) Neuromodulation and the orchestration of the respiratory rhythm. Respir Physiol Neurobiol 164:96-104.

Donlea JM, Alam MN, Szymusiak R (2017) Neuronal substrates of sleep homeostasis; lessons from flies, rats and mice. Curr Opin Neurobiol 44:228-235.

Engineer ND, Riley JR, Seale JD, Vrana WA, Shetake JA, Sudanagunta SP, Borland MS, Kilgard MP (2011) Reversing pathological neural activity using targeted plasticity. Nature 470:101-104.

Filosa A, Barker AJ, Dal Maschio M, Baier H (2016) Feeding State Modulates Behavioral Choice and Processing of Prey Stimuli in the Zebrafish Tectum. Neuron 90:596-608.

Freret T, Lelong-Boulouard V, Lecouflet P, Hamidouche K, Dauphin F, Boulouard M (2017) Co-modulation of an allosteric modulator of nicotinic receptor-cholinesterase inhibitor (galantamine) and a 5-HT4 receptor agonist (RS-67333): effect on scopolamine-induced memory deficit in the mouse. Psychopharmacology (Berl) 234:2365-2374.

Garcia VJ, Daur N, Temporal S, Schulz DJ, Bucher D (2015) Neuropeptide Receptor Transcript Expression Levels and Magnitude of Ionic Current Responses Show Cell Type-Specific Differences in a Small Motor Circuit. Journal of Neuroscience 35:6786-6800.

628 Goaillard JM, Taylor AL, Schulz DJ, Marder E (2009) Functional consequences of animal-to-
629 animal variation in circuit parameters. Nat Neurosci 12:1424-1430.
630 Golowasch J, Marder E (1992) Ionic currents of the lateral pyloric neuron of the stomatogastric
631 ganglion of the crab. J Neurophysiol 67:318-331.
632 Gray M, Daudelin DH, Golowasch J (2017) Activation mechanism of a neuromodulator-gated
633 pacemaker ionic current. J Neurophysiol 118:595-609.
634 He K, Huertas M, Hong SZ, Tie X, Hell JW, Shouval H, Kirkwood A (2015) Distinct Eligibility Traces
635 for LTP and LTD in Cortical Synapses. Neuron 88:528-538.
636 Hooper SL, Marder E (1987) Modulation of the lobster pyloric rhythm by the peptide proctolin. J
637 Neurosci 7:2097-2112.
638 Inagaki HK, Panse KM, Anderson DJ (2014) Independent, reciprocal neuromodulatory control of
639 sweet and bitter taste sensitivity during starvation in Drosophila. Neuron 84:806-820.
640 Li B, Beeman RW, Park Y (2011) Functions of duplicated genes encoding CCAP receptors in the
641 red flour beetle, Tribolium castaneum. J Insect Physiol 57:1190-1197.
642 Lovett-Barron M, Andalman AS, Allen WE, Vesuna S, Kauvar I, Burns VM, Deisseroth K (2017)
643 Ancestral Circuits for the Coordinated Modulation of Brain State. Cell 171:1411-1423
644 e1417.
645 Manor Y, Nadim F (2001) Synaptic depression mediates bistability in neuronal networks with
646 recurrent inhibitory connectivity. J Neurosci 21:9460-9470.
647 Marder E (2012) Neuromodulation of neuronal circuits: back to the future. Neuron 76:1-11.
648 Marder E, Bucher D (2007) Understanding circuit dynamics using the stomatogastric nervous
649 system of lobsters and crabs. Annual review of physiology 69:291-316.
650 McCormick DA, Pape HC (1990) Noradrenergic and serotonergic modulation of a
651 hyperpolarization-activated cation current in thalamic relay neurones. J Physiol 431:319-
652 342.
653 Mena W, Diegelmann S, Wegener C, Ewer J (2016) Stereotyped responses of Drosophila
654 peptidergic neuronal ensemble depend on downstream neuromodulators. Elife
655 5:e19686.
656 Mesce KA, Crisp KM, Gilchrist LS (2001) Mixtures of octopamine and serotonin have
657 nonadditive effects on the CNS of the medicinal leech. J Neurophysiol 85:2039-2046.
658 Mirabeau O, Joly JS (2013) Molecular evolution of peptidergic signaling systems in bilaterians.
659 Proc Natl Acad Sci U S A 110:E2028-2037.
660 Nadim F, Bucher D (2014) Neuromodulation of neurons and synapses. Curr Opin Neurobiol
661 29:48-56.
662 Nusbaum MP, Blitz DM, Marder E (2017) Functional consequences of neuropeptide and small-
663 molecule co-transmission. Nat Rev Neurosci 18:389-403.
664 Park JY, Spruston N (2012) Synergistic actions of metabotropic acetylcholine and glutamate
665 receptors on the excitability of hippocampal CA1 pyramidal neurons. J Neurosci
666 32:6081-6091.
667 Parker D (2000) Presynaptic and interactive peptidergic modulation of reticulospinal synaptic
668 inputs in the lamprey. J Neurophysiol 83:2497-2507.
669 Pena DF, Childs JE, Willett S, Vital A, McIntyre CK, Kroener S (2014) Vagus nerve stimulation
670 enhances extinction of conditioned fear and modulates plasticity in the pathway from
671 the ventromedial prefrontal cortex to the amygdala. Front Behav Neurosci 8:327.

672 Richter C, Woods IG, Schier AF (2014) Neuropeptidergic control of sleep and wakefulness. Annu
673 Rev Neurosci 37:503-531.
674 Schunn CD, Wallach D (2005) Evaluating Goodness-of-Fit in Comparison of Models to Data. In:
675 Psychologie der Kognition Reden und Vorträge anlässlich der Emeritierung von Werner
676 H. Tack: Saarbrücken Univ.-Präsidentin.
677 Shahidi R, Williams EA, Conzelmann M, Asadulina A, Veraszto C, Jasek S, Bezares-Calderon LA,
678 Jekely G (2015) A serial multiplex immunogold labeling method for identifying
679 peptidergic neurons in connectomes. Elife 4:e11147.
680 Smith NJ, Milligan G (2010) Allostery at G Protein-Coupled Receptor Homo- and Heteromers:
681 Uncharted Pharmacological Landscapes. Pharmacological Reviews 62:701-725.
682 Su J, Sandor K, Skold K, Hokfelt T, Svensson CI, Kultima K (2014) Identification and quantification
683 of neuropeptides in naive mouse spinal cord using mass spectrometry reveals [des-
684 Ser1]-cerebellin as a novel modulator of nociception. J Neurochem 130:199-214.
685 Svensson E, Grillner S, Parker D (2001) Gating and braking of short- and long-term modulatory
686 effects by interactions between colocalized neuromodulators. Journal of Neuroscience
687 21:5984-5992.
688 Swensen AM, Marder E (2000) Multiple peptides converge to activate the same voltage-
689 dependent current in a central pattern-generating circuit. J Neurosci 20:6752-6759.
690 Taghert PH, Nitabach MN (2012) Peptide neuromodulation in invertebrate model systems.
691 Neuron 76:82-97.
692 Thirumalai V, Marder E (2002) Colocalized neuropeptides activate a central pattern generator
693 by acting on different circuit targets. J Neurosci 22:1874-1882.
694 Thirumalai V, Prinz AA, Johnson CD, Marder E (2006) Red pigment concentrating hormone
695 strongly enhances the strength of the feedback to the pyloric rhythm oscillator but has
696 little effect on pyloric rhythm period. J Neurophysiol 95:1762-1770.
697 Tohidi V, Nadim F (2009) Membrane resonance in bursting pacemaker neurons of an oscillatory
698 network is correlated with network frequency. J Neurosci 29:6427-6435.
699 Tseng HA, Nadim F (2010) The membrane potential waveform of bursting pacemaker neurons is
700 a predictor of their preferred frequency and the network cycle frequency. J Neurosci
701 30:10809-10819.
702 van den Pol AN (2012) Neuropeptide transmission in brain circuits. Neuron 76:98-115.
703 Wester JC, McBain CJ (2014) Behavioral state-dependent modulation of distinct interneuron
704 subtypes and consequences for circuit function. Curr Opin Neurobiol 29:118-125.
705 White RS, Spencer RM, Nusbaum MP, Blitz DM (2017) State-dependent sensorimotor gating in a
706 rhythmic motor system. J Neurophysiol 118:2806-2818.
707 Woods IG, Schoppik D, Shi VJ, Zimmerman S, Coleman HA, Greenwood J, Soucy ER, Schier AF
708 (2014) Neuropeptidergic signaling partitions arousal behaviors in zebrafish. J Neurosci
709 34:3142-3160.
710 Xia XB, Mills SL (2004) Gap junctional regulatory mechanisms in the AII amacrine cell of the
711 rabbit retina. Vis Neurosci 21:791-805.
712 Yamazoe-Umemoto A, Fujita K, Iino Y, Iwasaki Y, Kimura KD (2015) Modulation of different
713 behavioral components by neuropeptide and dopamine signalings in non-associative
714 odor learning of Caenorhabditis elegans. Neurosci Res 99:22-33.

715 Zhao S, Sheibanie AF, Oh M, Rabbah P, Nadim F (2011) Peptide neuromodulation of synaptic
716 dynamics in an oscillatory network. J Neurosci 31:13991-14004.

717

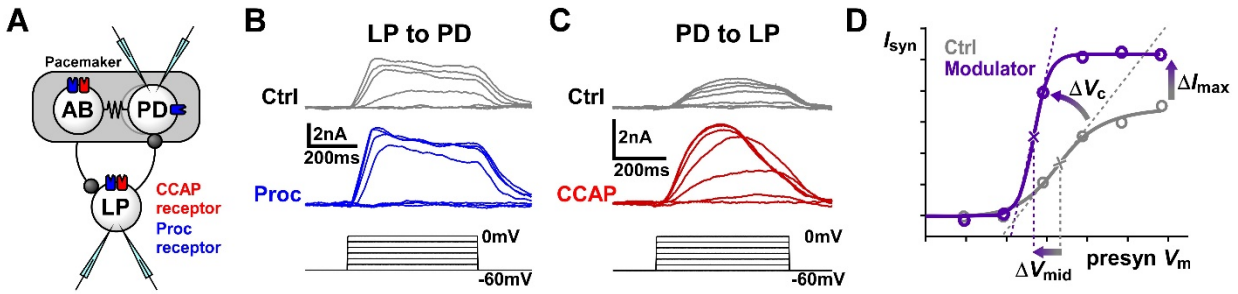

Figure 1. CCAP and Proc modulate the strength and activation curves of the reciprocal synapses between the LP and PD neurons. **(A)** Schematic diagram of the synaptic connectivity between the electrically-coupled (resistor symbol) pyloric pacemaker neurons, AB and PD, and the follower LP neuron. Both synapses (stick-and-ball symbols) are inhibitory. Also shown are the known receptor expressions for CCAP and putative receptor expressions for Proc in these neurons. The experimental protocol involved two-electrode recordings of the PD and LP neurons. **(B)** Example recordings of postsynaptic currents measured in the PD neuron in response to voltage steps in the presynaptic LP neuron in control saline (Ctrl) and in the presence of 1 µM Proc. Measurements were done in 0.1 µM TTX. **(C)** Example recordings of synaptic currents measured in the LP neuron in response to voltage steps in the presynaptic PD neuron in control saline (Ctrl) and in the presence of 1 µM CCAP. Measurements were done in 0.1 µM TTX. **(D)** To measure the modulatory effects, the mean value of the postsynaptic currents was plotted vs. the presynaptic voltage and fit with a Boltzmann type sigmoidal function. Changes in maximum synaptic current (I_{max}), the half-activation voltage (V_{mid}) and the slope factor (V_c) were compared in Ctrl and in the presence of the modulator.

Figure 2. CCAP and Proc modulate the synapses between the LP and PD neurons in a dose-dependent manner. **(A)** Both CCAP and Proc increase the amplitude of the LP to PD postsynaptic current (I_{syn}). Top panels show mean and SEM of I_{syn} as well as sigmoidal fits for control and modulators applied at the maximum concentration of 1 µM. As the applied concentration is increased, CCAP increases I_{max} ($p<0.0001$), decreases the slope factor V_c ($p<0.001$) and decreases V_{mid} ($p<0.0001$). (All tests One-Way RM-ANOVA, N=5.) Proc has a similar effect on these three parameters ($p<0.0001$ for I_{max} and V_c, $p=0.0047$ for V_{mid}, One-Way RM-ANOVA, N=6). **(B)** As the applied concentration increases, CCAP, but not Proc, increases the amplitude of the PD to LP synapse. Top panels as in A. CCAP increases I_{max} ($p<0.0001$), but not V_{mid} ($p=0.50$) or V_c ($p=0.95$), Proc modulates V_c ($p<0.0001$) but not I_{max} ($p=0.22$) or V_{mid} ($p=0.11$). All tests One-Way RM-ANOVA, N=6. (** $p<0.01$, *** $p<0.001$). All raw data are provided in Figure 2–source data.

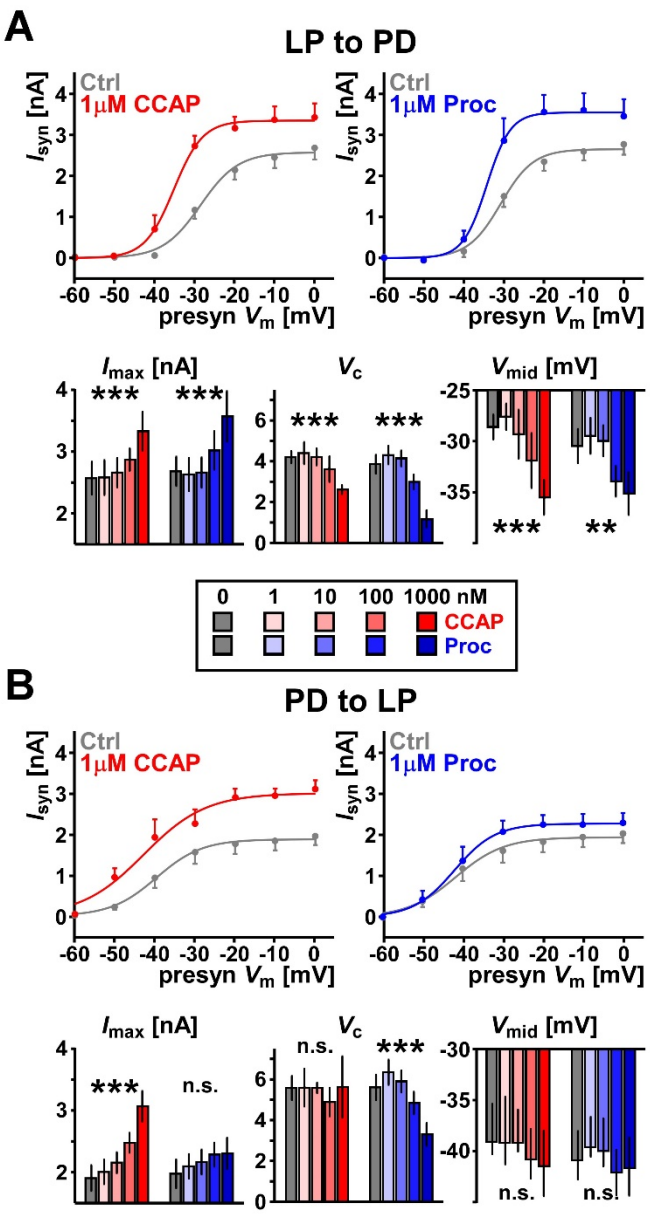

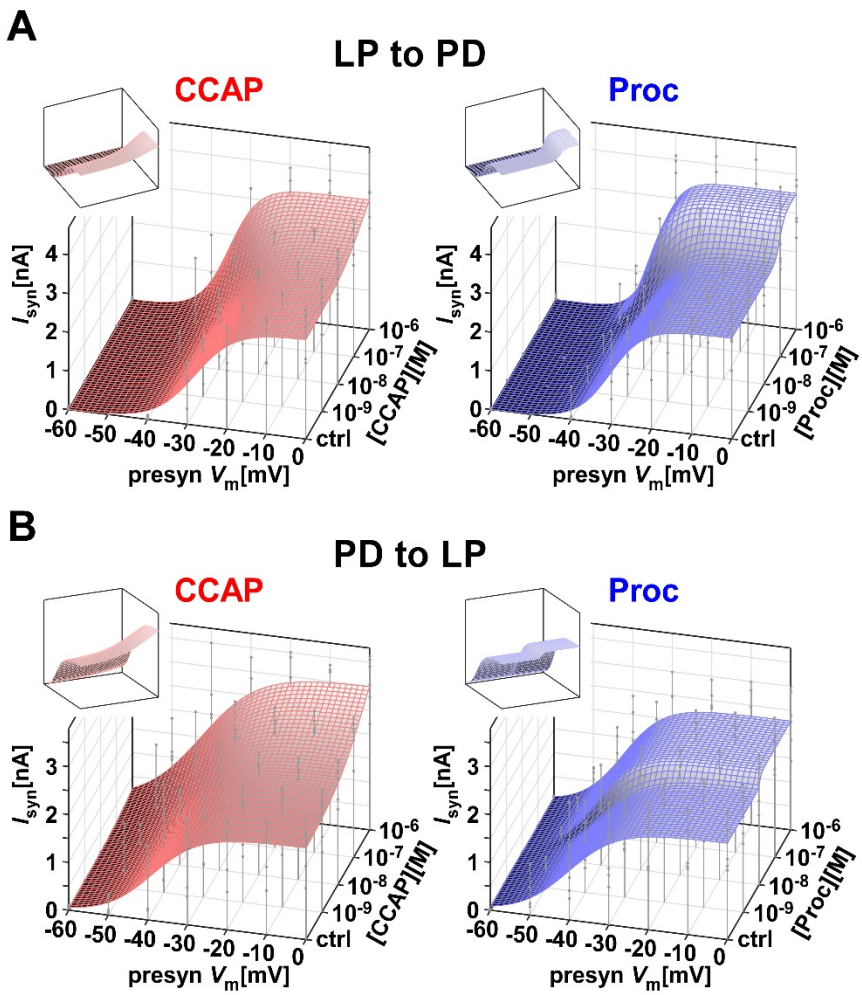

Figure 3. The dose-dependent influence of CCAP and Proc on the activation curves of the two synapses was used to construct predictors of modulation on synapses. **(A)** A double-sigmoidal surface fit (equation (3)) to the activation data of the LP to PD synapse in different doses of Proc or CCAP can be used to estimate the influence of the respective modulator on the synapse at any presynaptic voltage and any concentration of the modulator. Droplines indicate measurement points of the experimental data, with the filled circles marking the data points. Insets show the same surface from a different viewpoint. (B) Same as A, but for the PD to LP synapse. The fit parameters were: panel A, CCAP: a1=3.619, a2=-1.042, a3=-38.00, a4=9.890, a5=3.197, a6=1.920, C_{mid}=-6.556, C_c=0.5555; panel A, Proc: a_1=3.508, a_2=-0.902, a_3=-34.68, a_4=4.320, a_5=2.913, a_6=1.324, C_{mid}=-7.018, C_c=0.1359; panel B, CCAP: a_1=3.632, a_2=-1.735, a_3=-44.74, a_4=5.82, a_5=8.135, a_6=-2.116, C_{mid}=-6.455, C_c=0.8039; panel B, Proc: a_1=2.273, a_2=-0.2560, a_3=-42.43, a_4=2.090, a_5=5.184, a_6=1.126, C_{mid}=-7.958, C_c=0.04605.

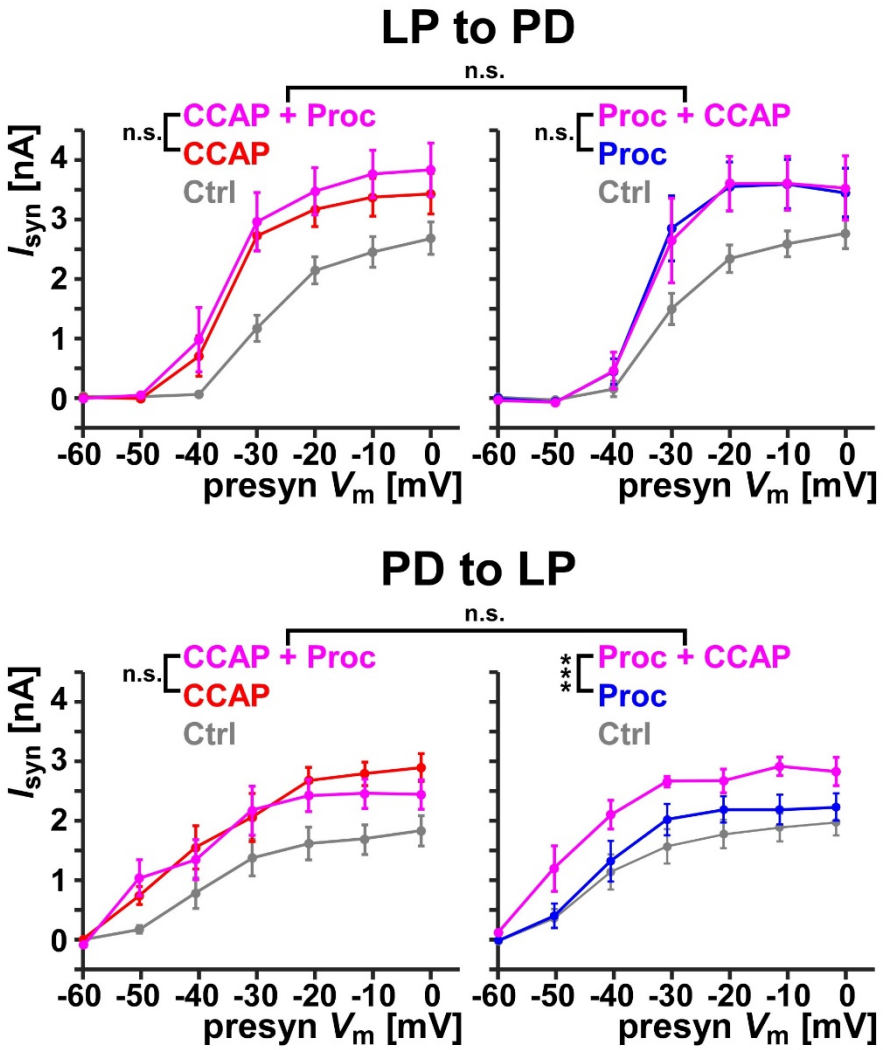

Figure 4. Maximum co-modulation of the synaptic currents by 1 µM CCAP and 1 µM Proc. Each panel shows the effect of co-modulation of either synapse on the synaptic activation curve, following modulation by 1 µM of either modulator alone. For the LP to PD synapse (top), co-modulation did not increase the synaptic current significantly compared to either CCAP alone (left, p=0.45, N=5) or Proc alone (right, p=1.0, N=6). Between the two sets of experiments (left and right panels), neither control levels (p=0.55), nor co-modulation levels (p=0.68) were significantly different. For the PD to LP synapse (bottom), co-modulation did not increase the synaptic current significantly compared to CCAP alone (left, p=0.99, N=6), but it did increase the effect of Proc alone (right, p <0.0001, N=6). Once again, between the two sets of experiments (left and right panels), neither control levels (p=0.73), nor co-modulation levels (p=0.47) were significantly different. All statistical comparisons were Two-Way RM-ANOVA, followed by a Tukey post hoc analysis, if applicable. (* p<0.05, *** p<0.001).

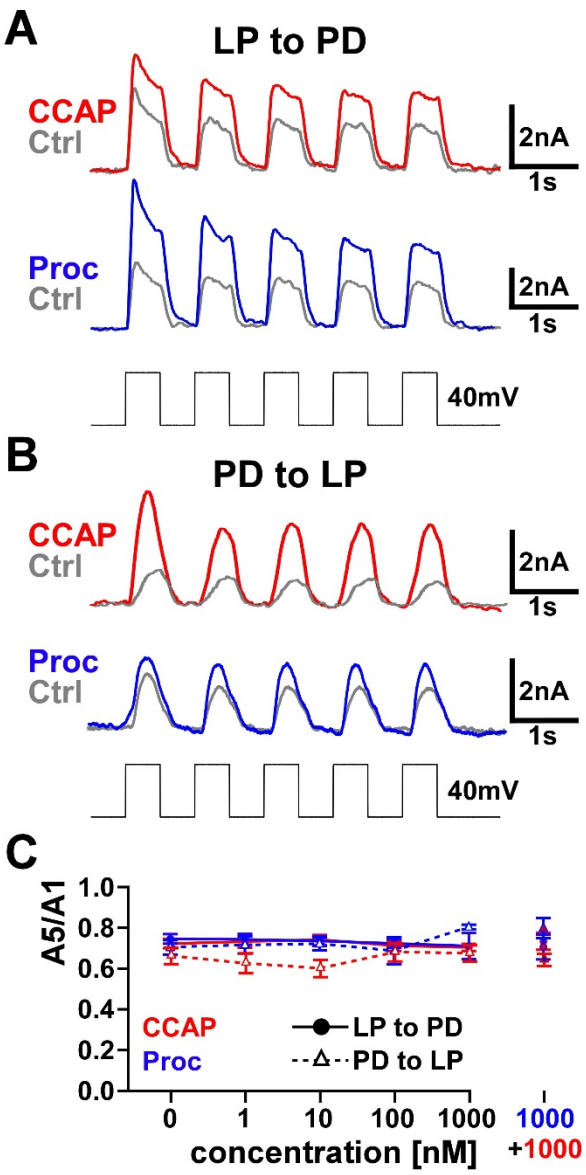

Figure 5. CCAP, Proc or both do not modulate short-term synaptic plasticity measured with 40 mV presynaptic voltage pulses. **(A, B)**: Sample experimental traces showing the five postsynaptic currents (with mean amplitude Amp1-Amp5) in response to a set of five presynaptic voltage pulses from -60 mV to -20 mV in control and in the presence of either modulator, for the LP to PD (**A**) and PD to LP (**B**) synapses. **(C)** Short-term synaptic plasticity was quantified as Amp5/Amp1. This ratio did not change from control to different concentrations of individual neuromodulators, or co-modulation. (LP to PD: from control to either CCAP or Proc to co-modulation, p=0.50 and 0.34. PD to LP: from control to either CCAP or Proc to co-modulation, p=0.20 and 0.11. N=6 for all. All measurements One-Way RM ANOVA).

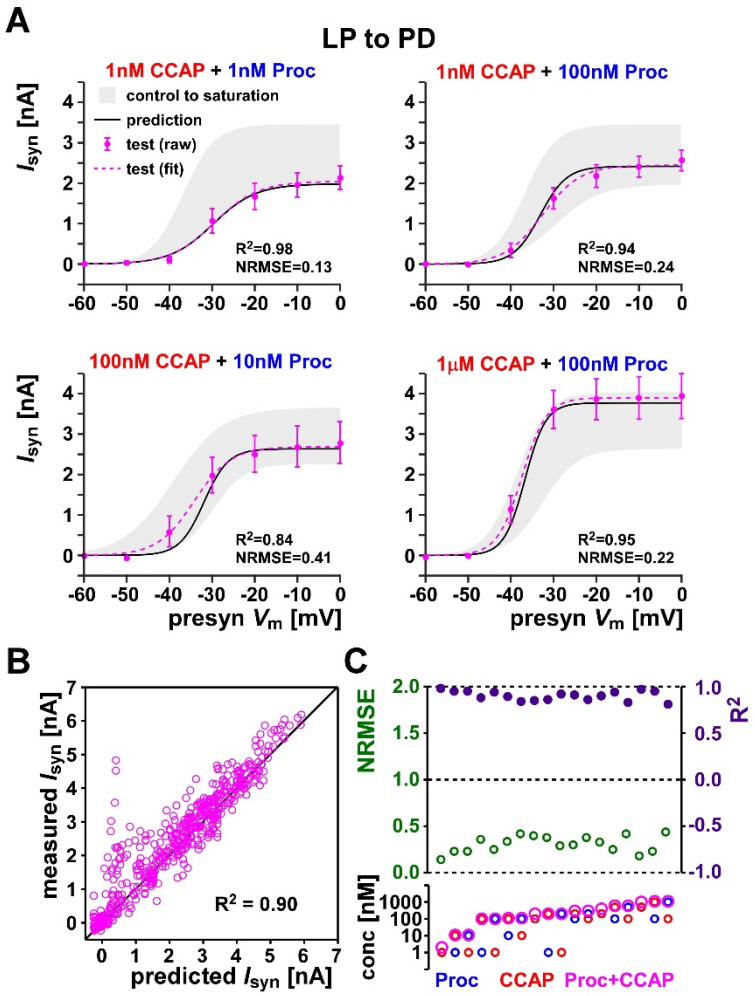

Figure 6. The co-modulatory effect of CCAP and Proc on the LP to PD synapse is predictable by a linear-summation-up-to-saturation model. **(A)** The LP to PD synaptic current activation curve in response to co-applied CCAP and Proc at four different concentration combinations (test, raw and fit) is well predicted by the model (prediction). Also shown is the range of synaptic currents measured in the respective experiments (control to saturation). The R^2 and NRMSE values in each case show the goodness of the prediction. **(B)** The prediction values compared with the actual measurements for all data points in the 18 different combinations of co-modulation measurements of the LP to PD synapse. Also shown, for comparison, are the line of perfect prediction (y=x) and overall R^2 values. All data points are provided in Figure 6–source data. **(C)** The R^2 and NRMSE values shown for each of the 18 co-modulation combinations of the LP to PD synapse. R^2=1 and NRMSE=0 indicate perfect predictions, whereas R^2=0 and NRMSE=1 indicate that the prediction was no better than the mean of the data. The bottom panel shows the concentration of Proc, CCAP and total concentration (Proc+CCAP) in each case. Data are shown in increasing order of total concentration. Each combination included 5-6 preparations.

Group	Proc [M]	CCAP [M]	R^2	NRMSE
1	10^{-9}	10^{-9}	0.98	0.13
2	10^{-9}	10^{-8}	0.95	0.22
2	10^{-9}	10^{-7}	0.88	0.35
2	10^{-9}	$2x10^{-7}$	0.86	0.37
1	10^{-8}	10^{-9}	0.95	0.22
3	10^{-8}	10^{-9}	0.95	0.22
1	10^{-7}	10^{-9}	0.94	0.24
4	10^{-7}	10^{-8}	0.84	0.41
3	10^{-7}	10^{-7}	0.85	0.39
4	10^{-7}	$2x10^{-7}$	0.91	0.29
4	10^{-7}	$5x10^{-7}$	0.94	0.24
4	10^{-7}	10^{-6}	0.95	0.22
1	$2x10^{-7}$	10^{-9}	0.92	0.28
3	$2x10^{-7}$	10^{-7}	0.86	0.37
1	$2x10^{-7}$	$2x10^{-7}$	0.90	0.32
3	$5x10^{-7}$	10^{-7}	0.83	0.41
2	$5x10^{-7}$	$5x10^{-7}$	0.97	0.17
3	10^{-6}	10^{-7}	0.81	0.43
All Data			**0.90**	**0.31**

Figure 6 - Figure supplement. Statistics of the LP to PD synapse co-modulation. Co-applications with the same Group number were performed in the same experiments.

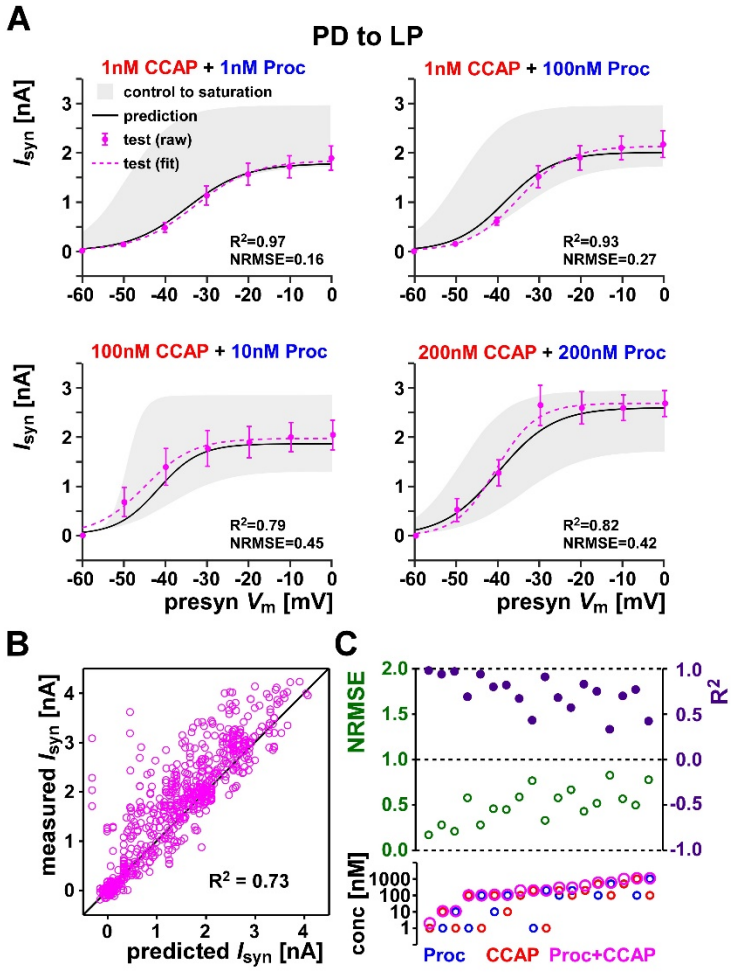

Figure 7. The co-modulatory effect of CCAP and Proc on the PD to LP synapse is predictable by a linear-summation-up-to-saturation model. **(A)** The PD to LP synaptic current activation curve in response to co-applied CCAP and Proc at four different concentration combinations (test, raw and fit) is well predicted by the model (prediction). Also shown is the range of synaptic currents measured in the respective experiments (control to saturation). The R^2 and NRMSE values in each case show the goodness of the prediction. **(B)** The prediction values compared with the actual measurements for all data points in the 18 different combinations of co-modulation measurements of the PD to LP synapse. Also shown, for comparison, are the line of perfect prediction (y=x) and overall R^2 values. All data points are provided in Figure 7–source data. **(C)** The R^2 and NRMSE values shown for each of the 18 co-modulation combinations of the LP to PD synapse. R^2=1 and NRMSE=0 indicate perfect predictions, whereas R^2=0 and NRMSE=1 indicate that the prediction was no better than the mean of the data. The bottom panel shows the concentration of Proc, CCAP and total concentration (Proc+CCAP) in each case. Data are shown in increasing order of total concentration. Each combination included 5-6 preparations.

Group	[Proc] (M)	[CCAP] (M)	R^2	NRMSE
1	10^{-9}	10^{-9}	0.97	0.16
2	10^{-9}	10^{-8}	0.93	0.27
2	10^{-9}	10^{-7}	0.68	0.57
2	10^{-9}	$2x10^{-7}$	0.42	0.76
1	10^{-8}	10^{-9}	0.96	0.20
3	10^{-8}	10^{-9}	0.79	0.45
1	10^{-7}	10^{-9}	0.93	0.27
4	10^{-7}	10^{-8}	0.81	0.44
3	10^{-7}	10^{-7}	0.66	0.58
4	10^{-7}	$2x10^{-7}$	0.67	0.57
4	10^{-7}	$5x10^{-7}$	0.74	0.51
4	10^{-7}	10^{-6}	0.76	0.49
1	$2x10^{-7}$	10^{-9}	0.90	0.32
3	$2x10^{-7}$	10^{-7}	0.56	0.66
1	$2x10^{-7}$	$2x10^{-7}$	0.82	0.42
3	$5x10^{-7}$	10^{-7}	0.32	0.82
2	$5x10^{-7}$	$5x10^{-7}$	0.69	0.56
3	10^{-6}	10^{-7}	0.41	0.77
All Data			**0.73**	**0.52**

Figure 7 - Figure supplement. Statistics of the PD to LP synapse co-modulation. Co-applications with the same Group number were performed in the same experiments.

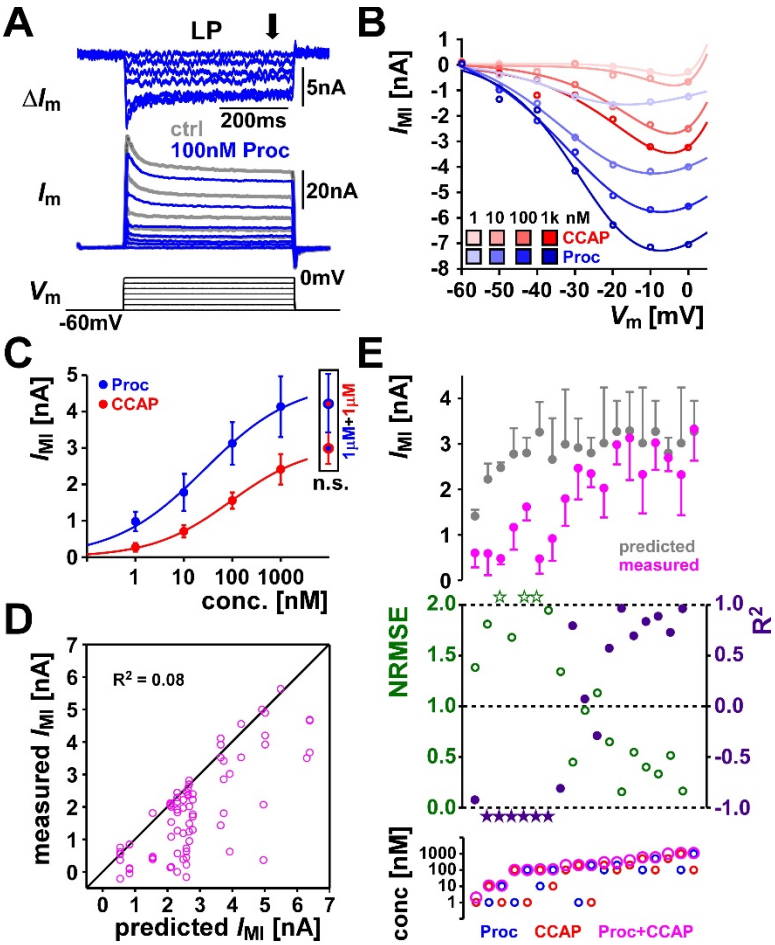

Figure 8. The co-modulatory effect of CCAP and Proc on the levels of I_{MI} in the LP neuron cannot be predicted by a linear-summation-up-to-saturation model. **(A)** Measurement of I_{MI} in the LP neuron. The total membrane current (I_m) was measured in the LP neuron, with 500 ms voltage steps from -60 to 0 mV, in control saline and in the presence of 100 nM Proc. The difference current (ΔI_m) was calculated by digital subtraction and I_{MI} was calculated as the mean current in the latter half of the voltage step (arrow). **(B)** Example of the I_{MI} IV curves measured in two experiments in increasing concentrations of CCAP or Proc, shown together with the fit of the data points using equation (2). **(C)** Dose-dependent levels of I_{MI} (measured at -15 mV) in the presence of Proc, CCAP or both (1 µM of each). Dose-dependent parameters, for CCAP: I_{max}= 3.080, C_{mid}= -7.025, C_c= 0.7997; for Proc: I_{max}=4.797, C_{mid}= -7.568, C_c= 0.8699. I_{MI} measured with co-applied 1 µM CCAP and Proc in the two sets of the experiments were not significantly different (Student's t-test, p = 0.31, N=6 for both sets of experiments.) **(D)** The linear-summation-up-to-saturation prediction values compared with the actual measurements of I_{MI} for all data points in the 18 different combinations of co-modulation. Also shown, for comparison, are the line of perfect prediction (y=x) and overall R^2 values. All data points are provided in Figure 8–source data. **(E)** Measured (at -15 mV) and predicted I_{MI} values, as well as the R^2 and NRMSE values shown for each of the 18 co-modulation combinations. R^2=1 and NRMSE=0 indicate perfect predictions, whereas R^2=0 and NRMSE=1 indicate that the prediction was no better than the mean of the data. Stars indicate out of range values. The bottom panel shows the concentration of Proc, CCAP and total concentration (Proc+CCAP) in each case. Data are shown in increasing order of total concentration. Each combination included 4-5 preparations.

Group	[Proc] (M)	[CCAP] (M)	R^2	NRMSE
1	10^{-9}	10^{-9}	-0.92	1.38
2	10^{-9}	10^{-8}	-62.69	7.98
2	10^{-9}	10^{-7}	-4.03	2.24
2	10^{-9}	$2x10^{-7}$	0.08	0.96
1	10^{-8}	10^{-9}	-2.27	1.81
3	10^{-8}	10^{-9}	-2.78	1.94
1	10^{-7}	10^{-9}	-1.82	1.68
4	10^{-7}	10^{-8}	-20.03	4.59
3	10^{-7}	10^{-7}	-0.80	1.34
4	10^{-7}	$2x10^{-7}$	0.57	0.65
4	10^{-7}	$5x10^{-7}$	0.83	0.41
4	10^{-7}	10^{-6}	0.97	0.17
1	$2x10^{-7}$	10^{-9}	0.79	0.45
3	$2x10^{-7}$	10^{-7}	-0.29	1.13
1	$2x10^{-7}$	$2x10^{-7}$	0.97	0.16
3	$5x10^{-7}$	10^{-7}	0.69	0.55
2	$5x10^{-7}$	$5x10^{-7}$	0.89	0.34
3	10^{-6}	10^{-7}	0.73	0.52
All Data			**0.08**	**0.96**

Figure 8 - Figure supplement. Statistics of the I_{MI} co-modulation. Co-applications with the same Group number were performed in the same experiments.

873